Implications of carbon saturation model structure for simulated nitrogen mineralization dynamics

Charles M. White[1*], Armen R. Kemanian[2], and Jason P. Kaye[1]

[1]Department of Ecosystem Science and Management
The Pennsylvania State University
116 Agricultural Sciences and Industries Building
University Park, PA 16802, USA

[2]Department of Plant Science
The Pennsylvania State University
116 Agricultural Sciences and Industries Building
University Park, PA 16802, USA

[*]Corresponding Author: cmw29@psu.edu

Abstract

Carbon (C) saturation theory suggests that soils have a limited capacity to stabilize organic C and that this capacity may be regulated by intrinsic soil properties such as clay concentration and mineralogy. While C saturation theory has advanced our ability to predict soil C stabilization, few biogeochemical ecosystem models have incorporated C saturation mechanisms. In biogeochemical models, C and nitrogen (N) cycling are tightly coupled, with C decomposition and respiration driving N mineralization. Thus, changing model structures from non-saturation to C saturation dynamics can change simulated N dynamics. In this study, we used C saturation models from the literature and of our own design to compare how different methods of modeling C saturation affected simulated N mineralization dynamics. Specifically, we tested (i) how modeling C saturation by regulating either the transfer efficiency (ε, g C retained g^{-1} C respired) or transfer rate (k) of C to stabilized pools affected N mineralization dynamics; (ii) how inclusion of an explicit microbial pool through which C and N must pass affected N mineralization dynamics; and (iii) whether using ε to implement C saturation in a model results in soil texture controls on N mineralization that are similar to those currently included in widely used non-saturating C and N models. Models were parameterized so that they rendered the same C balance. We found that when C saturation is modeled using ε, the critical C:N ratio for N mineralization from decomposing plant residues (r_{cr}) increases as C saturation of a soil increases. When C saturation is modeled using k, however, r_{cr} is not affected by the C saturation of a soil. Inclusion of an explicit microbial pool in the model structure was necessary to capture short term N immobilization-mineralization turnover dynamics during decomposition of low N residues. Finally, modelling C saturation by regulating ε led to similar soil texture controls on N mineralization as a widely used non-saturating model, suggesting that C saturation may be a

fundamental mechanism that can explain N mineralization patterns across soil texture gradients. These findings indicate that a coupled C and N model that includes saturation can (1) represent short-term N-mineralization by including a microbial pool and (2) express the effects of texture on N-turnover as an emergent property.

1. Introduction

Over the last two decades, the development of carbon (C) saturation theory has fundamentally changed our understanding of C storage in soils and new biogeochemical models have been developed to include C saturation dynamics (Hassink and Whitmore, 1997; Kemanian et al., 2005; Stewart et al., 2007; Kemanian et al., 2011). In biogeochemical models that couple C and nitrogen (N) cycles, C fluxes drive N mineralization (reviewed by Manzoni and Porporato, 2009). Thus, altering the structure of a C model to accommodate saturation dynamics is likely to affect the coupled N cycle. Yet, few attempts have been made to understand how C saturation affects N cycling (e.g. Castellano et al., 2012). In particular and to our knowledge, no study has addressed how the C saturation models proposed in the literature affect simulated N mineralization dynamics.

Carbon saturation theory suggests that soils have a limited capacity to stabilize organic C and that this capacity may be regulated by intrinsic soil properties such as clay concentration and mineralogy (Hassink, 1997; Six et al., 2002). Clay mineral surfaces stabilize and protect organic C through mineral organic complexes, leading to reduced C decomposition rates (Baldock and Skjemstad, 2000). As mineral surfaces in a soil become saturated with C, C decomposition rates increase, and the rate of soil organic C storage per unit of C input declines. This phenomenon results in an asymptotic response of soil organic C stocks to increasing C inputs (Stewart et al., 2007; Gulde et al., 2008; Heitkamp et al., 2012). Six et al. (2002) proposed a conceptual model of C protection based on measurable pools of organic C, including silt and clay associated C pools and particulate organic matter C pools. Several studies have indicated that the silt and clay associated C pools exhibit a saturating C storage response to increasing C inputs, while particulate organic matter increases linearly with C inputs (Gulde et al., 2008; Stewart et al.,

2008; Stewart et al., 2012). Given these findings, a new generation of ecosystem models which can simulate physicochemical stabilization of soil organic matter by mineral surfaces, among other processes, are needed to incorporate recent advances in our understanding of C cycling (Schmidt et al., 2011).

Despite the strong evidence for C saturation, the majority of ecosystem scale biogeochemical models that couple C and N cycles use linear C models with no saturation (reviewed by Manzoni and Porporato, 2009). Rothamsted C (Jenkinson, 1990) and Century (Parton et al., 1987) are two widely used non-saturating C models. In these models, C decomposition occurs with first-order kinetics and steady-state C levels will increase linearly as C inputs increase. In C saturation models, however, steady-state C levels will approach an asymptotic limit as C inputs increase. Both non-saturation and saturation C models couple N mineralization and immobilization ($N_{m\text{-}imm}$) to C decomposition (C_{dec}) through the C:N ratio (r) of any given pair of decomposing (r_{dec}) and receiving (r_{rec}) pools and the C transfer efficiency (ε, g C g^{-1} C) between pools (i.e. the proportion of decomposed C that is transferred to a receiving pool as organic C as opposed to being respired as CO_2, which is sometimes termed microbial growth efficiency). This coupling is represented as:

$$N_{m-imm} = C_{dec}\left(\frac{1}{r_{dec}} - \frac{\varepsilon}{r_{rec}}\right) \quad (1)$$

The coupling of C and N described by Eq. (1) expresses a relationship between C decomposition, C respiration, and N mineralization that will be affected by the structure of a C saturation model. For instance, one way to implement C saturation dynamics is by regulating ε as a function of the C saturation ratio (the ratio of the actual C to that of a putative maximum C level of the saturating pool, C_s/C_x) (Stewart et al., 2007; Kemanian et al., 2011) (Fig. 1a).

89 Alternatively, the transfer rate (k, T^{-1}) to the saturating pool can be regulated as a function of the
90 C saturation ratio (Hassink and Whitmore, 1997) (Fig. 1b). In both cases, when the saturation
91 ratio increases, ε and k effectively decrease because they are regulated multiplicatively by the
92 function $(1 - C_s/C_x)$ (Fig. 1). These two methods of implementing C saturation dynamics create
93 explicit couplings between C saturation and N mineralization dynamics in different ways, the
94 implications of which have not been explored.

95 The N mineralization in Eq. (1) applies to any transfer of C and N between pools. The
96 extent to which net N mineralization occurs as opposed to net N immobilization depends on the
97 magnitude of ε and the difference between r_{dec} and r_{rec}. The r of decomposing plant residue can
98 vary widely across residue types. The critical r (r_{cr}) below which decomposing residue will
99 cause positive net N mineralization can be solved using Eq. (1) when $N_{m\text{-}imm}=0$, as shown in Eq.
100 2.

$$r_{cr} = \frac{r_{rec}}{\varepsilon} \quad (2)$$

101 This equation shows that a decrease in ε will increase r_{cr}. For example, if the receiving pool is
102 saturated, the r_{cr} of decomposing substrates increases. The biological meaning of a decreasing ε
103 is that a smaller fraction of the products of microbial decomposition stabilize in organo-mineral
104 associations and thus remain available for further microbial decomposition. The r_{cr} in Eq. (2) is
105 for a single transfer and not for the sum of all transfers in a whole soil. A single transfer may
106 immobilize N while a simultaneous transfer among other pools in the soil may result in net N
107 mineralization at the whole soil level.

108 Although the coupling of C and N cycles in soils is largely mediated by microbial
109 biomass, the microbial pool has been given little consideration in saturation models. In only one
110 case is the microbial pool explicitly represented in the model structure (Hassink and Whitmore,

111 1997). This is in contrast to the body of contemporary C models in whole, where 60% of models
112 include one or more microbial pools (Manzoni and Porporato, 2009). In other C saturation
113 models, the microbial pool is either not included (Stewart et al., 2007) or is implicitly included
114 when parameterizing ε (Kemanian et al., 2011). In the latter model, ε lumps in one step what is a
115 cascade of C transfers among pools mediated by microbial turnover. While this approach may
116 produce reasonable results for net C exchange in monthly or yearly time frames, when these ε are
117 used for short time steps they may obscure the N cycling during microbial turnover.
118 A feature that implicitly links non-saturation and saturation C models is the role of soil
119 clay concentration (f_{clay}) in mediating ε, and hence N mineralization. In C saturation models, f_{clay}
120 is used to calculate the maximum size of the saturating pool (Hassink and Whitmore, 1997;
121 Kemanian et al., 2011), thus the C saturation ratio is a function of f_{clay}. Models that use the C
122 saturation ratio to regulate ε thus connect f_{clay} to ε. Non-saturating C cycling models have long
123 used f_{clay} to directly regulate ε (Parton et al., 1987; Jenkinson, 1990; Verberne et al., 1990) in a
124 way that leads to lower N mineralization rates and a lower r_{cr} in clay-rich soils. This method
125 originated from observations that soils with high f_{clay} stabilize a greater proportion of C inputs.
126 For example, Jenkinson (1990) and Parton et al. (1987) used relationships derived from Sørensen
127 (1975) and Sørensen (1981). However, Hassink (1996) found that the C saturation ratio of a soil
128 was a better predictor of C retention than f_{clay}, suggesting that C saturation may be a more
129 fundamental mechanism to integrate the effect of soil texture in a coupled C and N model.
130 Despite the commonalities in how f_{clay} controls N mineralization in both saturating and non-
131 saturating C models, the behavior of N mineralization in these two types of C models has never
132 been formally compared in the literature.

In summary, while N dynamics are mathematically linked to C cycling in all biogeochemical models, the implications of C saturation model structure for simulated N mineralization dynamics have not been addressed nor compared with that of non-saturation models. To advance the understanding of these areas we propose a set of hypotheses about how the structure and parameterization of different C models will affect the dynamics of a coupled N mineralization model. First, the method used to implement C saturation in a model, either through regulation of transfer efficiency (ε) or transfer rate (k), will affect N mineralization dynamics. Second, whether or not C saturation models include an explicit microbial pool through which C and N must pass will affect N mineralization dynamics. Finally, using ε to implement C saturation in a model results in soil texture controls on N mineralization that are similar to those currently included in widely used non-saturating C and N models. To test these hypotheses, we compared three different C saturation models and one non-saturation model (Fig. 2). These model structures were taken from the literature or developed for this investigation. Models varied in whether C saturation regulated either ε or k and whether a microbial pool was included in the saturation model. We coupled N to C cycling to obtain N mineralization and illustrate how the C model structure affects the r_{cr} and the temporal dynamics of a simulated inorganic N pool during plant residue decomposition.

2. Methods

2.1. Structure of the Carbon Models

We focused on three C saturation models with increasing complexity and one non-saturation C model (Fig. 2). The first and simplest model in our study is a single-pool saturation model, adapted from the models proposed by Kemanian et al. (2005, 2011) and Stewart et al.

156 (2007). The second model expands the single-pool saturation model by adding a microbial pool
157 (C_m). We termed this model the microbial saturation model to reflect the explicit inclusion of a
158 microbial pool through which C and N must pass. The third model is the abiotic saturation
159 model, whose structure was proposed by Hassink and Whitmore (1997). This model includes a
160 microbial pool (C_m), a labile unprotected pool (C_{un}), and a saturating pool of protected C (C_s).
161 We called this the abiotic saturation model because the saturating pool is directly linked to the
162 labile pool and any transfers are abiotic sorption and desorption. We compared these three C
163 saturation models to the Rothamsted C (RothC) model (Jenkinson, 1990), which is based on first
164 order kinetics and results in a linear relationship between C input and steady-state C level.
165 Because the main purpose of this study is to compare how the structure of C models
166 affects N mineralization, rather than C storage, we forced the turnover rate parameters so that
167 each model would return similar steady-state C stocks at a given level of fresh C inputs. We used
168 turnover rates from RothC as defaults and the resulting steady state soil C as a reference for other
169 models. A detailed description of each model is provided in the following sections. For
170 reference, model structures are diagrammed in Fig. 2, parameters are specified in Table 1, and
171 the differential equation for each pool is in Table 2.

172 **2.1.1. Single-pool Saturation Model**

173 In the single-pool saturation model, decomposed C from the pool of residue inputs (C_r) is
174 transferred directly to C_s. The ε from C_r to C_s is regulated by an efficiency factor (ε_x) and the
175 saturation ratio (C_s/C_x). We calculate C_x as a function of f_{clay} using the formula developed by
176 Hassink and Whitmore (1997). In this model, ε_x represents a humification coefficient (*sensu*
177 Hénin and Dupuis, 1945), or the slope that would be obtained by regressing dC_s/dt against C
178 inputs. This coefficient is an effective efficiency that lumps the C use efficiency of the microbes

feeding on residues and on microbial biomass (predation), detritus and exudates. We used ε_x = 0.18 g C g^{-1} C. This value is in the upper range reported by Huggins et al. (1998), and would correspond to three cycles of microbial feeding with a C use efficiency of 0.56 g C g^{-1} C (i.e., 0.56^3). This C use efficiency agrees well with a representative upper value in soils reported in Fig. 6 of Manzoni et al. (2012). Both C_r and C_s decay with first order kinetics according to the rate constants in Table 1. Decomposed C that is not transferred to C_s is respired as CO_2. The turnover rate of soil C (k_s) in this model is taken from RothC. The residue C pool turnover rate (k_r) in all three saturation models is taken as the weighted average of the turnover rates for decomposable (k_{dpm}) and resistant (k_{rpm}) plant material input pools in RothC (i.e., $0.59k_{dpm}+0.41k_{rpm}$).

2.1.2. Microbial Saturation Model

In the microbial saturation model, C decomposed from C_r and C_s is transferred to C_m while C decomposed from C_m is transferred to C_s. The ε from decomposing pools to receiving pools is calculated as the square root of the ε used in the single-pool saturation model. Thus, C that is stepping from C_r to C_m and from C_m to C_s is retained with an overall efficiency similar to the single-pool model. Decomposed C that is not transferred to a receiving pool is respired as CO_2. The three pools C_r, C_m, and C_s decay with first order kinetics. The turnover rate of the microbial pool (k_m) in this model is taken from RothC while k_s is derived to maintain a steady state C_s level that is equivalent to the single-pool saturation model. The derivation for k_s is provided in Appendix A.

2.1.3. Abiotic Saturation Model

The abiotic saturation model is adapted from the structure proposed by Hassink and Whitmore (1997). Decomposed C from C_r and C_{un} is transferred to C_m with a fixed ε representing microbial C use efficiency. Carbon in C_{un} is also transferred to C_s, a protected pool, simulating the abiotic sorption of organic C to mineral surfaces. The transfer rate from C_{un} to C_s ($k_{un\text{-}s}$) is controlled by a maximum rate that is regulated by the size of C_s relative to its maximum capacity (C_x), with the latter being calculated as a function of f_{clay} using the original linear regression developed by Hassink and Whitmore. Transfer of C from C_s to C_{un}, representing the desorption of organic C from the mineral phase, occurs at the rate k_s. Because the sorption-desorption process is abiotic, the ε between C_{un} and C_s is 1 (no CO_2 is respired in the transfer). The turnover rates k_r and k_m are consistent with the other saturation models. We set the default value for the decay rate k_{un} at 0.01 d^{-1} while the decay rates $k_{un\text{-}s}$ and k_s were derived such that steady state C_s level would be equivalent to the single-pool saturation model (see Appendix A for the derivation).

2.1.4. Rothamsted C Model

In the RothC model (Jenkinson, 1990), C pools include decomposable (C_{dpm}) and resistant (C_{rpm}) fractions of plant material inputs, and microbial (C_m) and stabilized (C_s) pools of soil C. Each pool decays with its own first-order rate constant. Decomposed C from each pool is transferred to the receiving pools with an efficiency (ε) that is determined by f_{clay}. This efficiency varies from a low of 0.15 at 0.01 clay concentration to a plateau of approximately 0.24 at 0.45 clay concentration. The fraction of decomposed C that is not transferred to a receiving pool (1- ε) is respired as CO_2. Of the total C decomposed from all pools and not lost as CO_2, 54% is transferred to C_s and 46% is transferred to C_m.

225

226 *2.2. Modeling N mineralization*

227 We coupled a simple N mineralization-immobilization model to each of the four C
228 models using the convention described in Eq. (1). The coupling of C and N for each model
229 structure is diagrammed in Fig. 2. In this N mineralization model, N decomposes from the donor
230 pool in proportion to C decomposition based on the r_{dec}. A portion of the decomposed C is
231 transferred to a receiving pool based on ε, while the remaining C is respired as CO_2.
232 Decomposed organic N is transferred to the receiving pool in proportion to the C received by the
233 pool based on the r_{rec}. Nitrogen mineralization (or immobilization) is calculated as the difference
234 between the N decomposed and the N assimilated by the receiving pool. Nitrogen mineralized as
235 a result of C decomposition is added to an inorganic N (N_i) pool. When $N_{m\text{-}imm}$ is negative,
236 immobilization occurs and N is removed from the N_i pool. If the pool size of N_i is insufficient to
237 meet the immobilization demand, C decomposition is limited by N availability, as we assume
238 that ε will not change. Under such circumstances, we calculate the reduced C decomposition by
239 rearranging Eq. (1) and assuming that $N_i + N_{m\text{-}imm} = 0$:

240

$$C_{dec} = \frac{N_i}{\frac{\varepsilon}{r_{rec}} - \frac{1}{r_{dec}}} \qquad (16)$$

241

242 We use a fixed *r* of 10 for the microbial and soil organic matter pools while the *r* of the input
243 residues was a variable parameter input to the model.

244 To maintain simplicity of our N model, we do not include N transformations such as
245 nitrification or N losses such as leaching and plant uptake. Thus, in time series modeling
246 exercises, the N_i pool represents the cumulative sum of net N mineralization and immobilization.

Due to the simplification of our N model, we do not include N cycling feedbacks on C cycling, which are known to exist in nature and are sometimes included in more sophisticated models (e.g. Schimel and Weintraub, 2003; Eliasson and Ågren, 2011)

2.3. Modeling Exercises

To study and illustrate the differences in C and N cycling among the four models and the implications of the C model structure on N mineralization we did the following: (i) derived the analytical solutions to the steady-state size of each C pool as a function of C input level for all models; (ii) calculated the r_{cr} for a range of f_{clay} and saturation ratios; and (iii) simulated the temporal dynamics of N mineralization at a daily time-step following a one-time residue addition.

In the daily time-step residue addition simulation, a 5 Mg C ha^{-1} mass of plant residues with a *r* of 60 added to the soil on day 1 was allowed to decompose for 365 days. Nitrogen mineralization and/or immobilization resulting from residue and soil organic matter decomposition was added to or removed from the N_i pool. The simulation was conducted for 0.05 clay concentration and 0.25 clay concentration soils. Soil organic C pool sizes in each model were initialized to steady-state levels for an annual plant residue addition level of 5 Mg C ha^{-1} (equations in Table 3). The N_i pool was initialized to a size of 0.05 Mg N ha^{-1} to prevent N limitation of decomposition during the modeling exercise. Simulations were conducted in Microsoft Excel using the Visual Basic for Applications programming language.

3. Results

3.1. Characteristics and Behavior of the C Models

As expected, steady-state levels of C pools in each model responded to increasing C inputs in either a saturating or linear manner based on the parameterization of each model structure (Table 3 and Fig. 3). The C_s pool saturates in all three saturation models and C_m saturates in the microbial saturation model. In the single-pool saturation and microbial saturation models, this results because the C transfer efficiency (ε) to C_s and C_m is regulated by the C saturation ratio. As C saturation increases, more C is respired as CO_2 in the transfer and less is retained by the receiving pool. The C_s pool saturates in the abiotic saturation model because $k_{un\text{-}s}$ is regulated by the C saturation ratio. As C saturation increases, less C is transferred from C_{un} to C_s. In the abiotic saturation model, C_m and C_{un} are non-saturating and respond linearly to increasing C inputs, as do all the pools in RothC. The linear response is because the ε to these pools is a fixed value. Increasing f_{clay} from 0.05 to 0.25 led to increased C storage in the C_s pools of all saturation models and RothC, and the C_m pools of the microbial saturation model and RothC (Fig. 3). In the abiotic saturation model, C_m and C_{un} levels were unaffected by f_{clay}.

When C input levels and soil clay concentration were low, only small differences in total C storage were predicted by each model, as calculated by summing the mass of all C pools (Fig. 3c and 3d). However, at higher C input levels and soil clay concentration, large divergences between the saturation models and RothC occurred owing to the asymptotic characteristic of saturation models. Even though the abiotic saturation model contained the non-saturating pools C_{un} and C_m, the overall response of total C storage to increasing C inputs was similar to that of a pure saturation model. This is because of the relatively small size of the C_{un} and C_m pools compared to C_s when C inputs are within the range typical of most ecosystems (<15 Mg C ha^{-1} y^{-1}).

293 *3.2. Nitrogen Mineralization Dynamics*

294 The method used to implement C saturation in a model, by regulating either transfer
295 efficiency (ε) or transfer rate (*k*), affected N mineralization dynamics. When C saturation is
296 implemented by regulating ε, as in the single-pool saturation and microbial saturation models,
297 the saturation ratio affects the r_{cr} of decomposing plant residues (Table 4, Fig. 4a). In these
298 models, r_{cr} increases as the saturation ratio increases. On the other hand, when C saturation is
299 implemented by regulating *k*, as in the abiotic saturation model, r_{cr} is independent of the
300 saturation ratio (Table 4, Fig. 4a).

301 The explicit inclusion of a microbial pool in the C saturation models also affected N
302 mineralization dynamics. When a microbial pool was not explicitly included, as in the single-
303 pool saturation model, r_{cr} ranged from 55 to nearly 1,000 over the saturation ratio gradient (Fig.
304 4a). In the microbial saturation and abiotic saturation models, where C and N flow through a
305 microbial pool, r_{cr} was lower and had a narrower range over the saturation ratio gradient. In the
306 microbial saturation model, r_{cr} ranged from 25 to 200 over the saturation ratio gradient while the
307 abiotic saturation model had a fixed r_{cr} of 40 (Figure 4a). The inclusion of a microbial pool also
308 affected the temporal dynamics of N mineralization during simulated residue decomposition. In
309 the microbial saturation and abiotic saturation models, decomposition of plant residue with r=60
310 led to an initial period of net N immobilization, whereas the single-pool saturation model
311 predicted immediate net N mineralization (Fig. 5).

312 Using ε to implement C saturation in the single-pool saturation and microbial saturation
313 models led to soil texture controls on N mineralization that were similar to RothC, a widely used
314 non-saturating model. In these three models, r_{cr} decreased as clay concentration increased (Fig.
315 4b). The r_{cr} in RothC decreased from 59 at a clay concentration of 0.05 to 41 at a clay

316 concentration of 0.80. Across the same clay concentration gradient, r_{cr} in the single-pool
317 saturation model decreased from 86 to 66 and r_{cr} in the microbial saturation model decreased
318 from 29 to 26.
319
320 **4. Discussion**
321 A significant result from our work is that despite similar predictions of C storage across
322 the saturation models, dynamics of N mineralization diverged widely due to the structure of each
323 model. We revealed two important considerations for how C saturation models can be linked to
324 N mineralization dynamics. First, the influence of C saturation on N mineralization dynamics
325 depends on whether C saturation is modeled as a process regulating transfer efficiencies or a
326 process regulating transfer rates. Second, a single-pool C saturation model that may predict
327 long-term C storage well can misrepresent short-term N mineralization if N cycling is simply
328 linked to the long cadence of C cycling. For example, the single-pool C saturation model
329 predicted N mineralization from high *r* ratio litter inputs ($r > 60$) which normally result in N
330 immobilization (Manzoni et al., 2008; Sinsabaugh et al. 2013). This mismatch between C and N
331 cycling can be greatly improved by simply adding an intermediate pool of microbial biomass
332 through which C and N must pass; an addition that does not affect long term C cycling. Finally,
333 we demonstrated that soil texture controls on N mineralization can be similar between saturation
334 and non-saturation models. These findings have important implications about how the structure
335 of C saturation models affect N mineralization and offer new hypotheses about the links between
336 C saturation and N mineralization processes that should be tested with further research, as
337 described in the following sections.
338 **4.1. Regulating ε vs. *k* to implement C saturation affects N mineralization dynamics**

The influence of C saturation on N mineralization dynamics depends on whether C saturation is modeled as a process regulating ε or *k*. In the single-pool and microbial saturation models, the C saturation ratio is used to regulate ε, coupling C saturation and N mineralization processes based on Eq. (1). In the abiotic saturation model, where the saturation ratio does not regulate ε but rather *k*, C saturation does not affect N mineralization dynamics. These differences in how the models simulate C saturation present contrasting hypotheses of how C saturation could affect N mineralization dynamics.

If C saturation does affect N mineralization, there may be important implications for ecosystem management. For example, increasing C inputs to an ecosystem to promote C sequestration, or large disposals of manure in the soil, would move the soil closer to C saturation, causing more N mineralization from the inputs and potentially increased N losses. Management practices that redistribute SOC concentrations in a soil profile and mix layers with higher saturation ratio (e.g. top layer in no-till systems) with layers of lower saturation, would result in altered N mineralization patterns from crop residues.

A limited number of studies addressed these potential implications. Castellano et al. (2012) presented a conceptual model linking C and N saturation theories which was supported by evidence that increasing levels of C saturation reduced the transfer of NH_4-N to mineral associated organic matter and increased potential net nitrification. Similarly, McLauchlan (2006) found that net N mineralization decreased as clay concentration increased in soils aggrading C following agricultural abandonment. The findings of both of these studies are consistent with the behavior of a C saturation model where the C saturation ratio regulates ε. In such a model, increasing C saturation would reduce ε, resulting in less N immobilization (as in Castellano et al., 2012) or greater N mineralization (as in McLauchlan, 2006).

4.2. Inclusion of a microbial pool in C saturation models affects N mineralization dynamics

In order to obtain reasonable predictions of N mineralization from decomposing plant residues, it was necessary to include an explicit microbial pool in the C saturation model. In the single-pool saturation model, an explicit microbial pool is not included, rather an effective C transfer efficiency between C_r and C_s lumps approximately three cycles of microbial predation into one step. This approach has been used to accurately predict C storage over decadal time scales (Kemanian and Stöckle, 2010) and a single-pool model offers the advantages of parsimony (Stewart et al., 2007) and simplicity of calibration requirements (Kemanian and Stöckle, 2010). However, when coupled to a model of N mineralization, the single-pool saturation model yielded a r_{cr} that ranged from 55 to over 555 as the C saturation ratio rose above 0.9 (Fig. 4a). This range of r_{cr} is above the range that has been observed across a variety of ecosystem and substrate types except for woody residue substrates (Manzoni et al., 2008).

The steepness of the rise in r_{cr} as C saturation ratio increases in the single-pool model could be tempered by exponentiating the C saturation ratio. For example, Kemanian et al. (2011) raised the C saturation ratio to the sixth power. While this method may maintain r_{cr} at more reasonable levels across a broader range of C saturation ratios, it only shifts the sharp rise in r_{cr} to a higher saturation ratio and accentuates the steepness of the rise when it does occur.

In the single-pool model, the steep rise in r_{cr} as C saturation increases is unrealistic. A simple modification, adding an intermediate pool representative of microbial biomass, greatly improved the dynamics of N mineralization in the microbial saturation model. In this model, r_{cr} ranged from 23 to over 74 as the C saturation ratio rose above 0.9 (Fig. 4a). A similar range of r_{cr} values was observed in non-woody plant residues by Manzoni et al. (2010), though the range

was mostly explained by N concentration of the residues rather than C saturation of the soil. Within C saturation ratios that would occur under a more realistic C input level (~5 Mg C ha^{-1} y^{-1}), the r_{cr} in the microbial saturation model ranged narrowly from 26 to 29 across a range of clay concentrations (Fig. 4b). The abiotic saturation model predicted an r_{cr} of 40 based on a fixed microbial growth efficiency (ε) of 0.25. The r_{cr} predicted by the two C saturation models with explicit microbial pools fall closely in line with traditional estimates of r_{cr} that have been developed for relatively N rich residues (Sinsabaugh et al., 2013).

Compared to a single pool saturation model, the addition of a microbial pool to a C saturation model allows representing the short-term dynamics of N storage and turnover in microbial biomass. This improvement is achieved while preserving estimates of C storage and at the cost of only one additional parameter to the model. This improvement results in a model structure that can be applied to a broader set of ecological processes including both C and N cycling at short and long time scales.

4.3. Soil texture controls on N mineralization can be similar between saturation and non-saturation models

Soil texture has direct and indirect regulating effects on ε in RothC, the single-pool saturation and microbial saturation models, resulting in similar soil texture controls on N mineralization among the saturation and non-saturation models. RothC uses f_{clay} to directly regulate ε while the single-pool saturation and microbial saturation models use f_{clay} to regulate C_x, thus affecting ε (Table 1). In all three of these models, r_{cr} decreases with increasing clay concentration when the pool size for C_s is maintained constant (Fig. 4b). This occurs because a greater fraction of C and N are transferred to stabilized pools in clay rich soils rather than being mineralized. Early studies that demonstrated soil texture controls on N mineralization under a

paradigm of non-saturation C models (Ladd et al., 1981; Van Veen et al., 1985; Schimel, 1986) are consistent with the behavior of C saturation models that use ε to implement saturation. Therefore, C saturation theory may provide a mechanism to explain the effects of soil texture on C and N cycling.

4.4 Relevance to ecosystem processes and future research

Although the currently limited data on the links between C saturation and N mineralization dynamics seem to support a coupling of these processes (Castellano et al., 2012), it does not permit assessing with certainty the practical significance of such a relationship. For instance, at reasonable C input rates, the change in r_{cr} due to the effects of a clay gradient on the C saturation ratio is rather minor in the microbial saturation model (e.g., 26 to 29 as in Fig. 4b). The effect of C saturation on r_{cr} becomes much more pronounced as the saturation ratio increases above 0.5 (Fig. 4a). This level of saturation requires high C inputs per unit of soil mass under the current parameterization of our model, but can be achieved in the top layer of undisturbed no-till agricultural soils or pasture lands (Mazzilli et al., 2014) or in low clay concentration soils (Castellano et al., 2012).

Given the limited but encouraging data supporting the conceptual and quantitative link between C saturation and N mineralization, we believe that further empirical research should be pursued to test the hypothesis that C saturation is a mechanism that controls N mineralization. In testing this hypothesis, it will be particularly important to design studies that utilize C saturation gradients across similar soil textures, as one can argue that it is difficult to separate saturation from clay concentration effects in the experiments reported in the literature (Ladd et al., 1981; Van Veen et al., 1985; Schimel, 1986; McLauchlan, 2006; Castellano et al., 2012). A more specific hypothesis generated by our work is that as C saturation ratio increases so does the r_{cr} of

431 decomposing plant residues. If this hypothesis is correct, further studies should evaluate its
432 practical implications for managing C and N in natural and managed ecosystems. For example, a
433 hypothesis for an applied field experiment might be that N mineralization dynamics are altered
434 by C saturation patterns occurring in soil profiles with stratified soil organic matter, such as those
435 in no-till agricultural systems. We also suggest conducting additional studies to verify and
436 improve our estimation of the maximum soil C storage capacity (C_x), as the quantitative
437 relationship between C saturation and N mineralization is sensitive to this value and our current
438 method of estimation is based on the results of only one study (Hassink and Whitmore, 1997).
439 Recent advances in the understanding of C cycling, including C saturation theory, need to
440 be incorporated into a new generation of ecosystem models (Schmidt et al., 2011, but see
441 Kemanian and Stöckle, 2010; Kemanian et al., 2011). Along with C saturation, others are active
442 in incorporating microbial priming effects (Wutzler and Reichstein, 2008; Perveen et al., 2014)
443 and controls on microbial C use efficiency (Allison et al., 2010; Wetterstedt and Ågren, 2011)
444 into biogeochemical models. Perveen et al. (2014) demonstrated that N cycling was affected by
445 increased fresh C inputs from elevated CO_2 in a priming effect model. Interestingly, the
446 definition for microbial priming proposed by Wutzler and Reichstein (2008), where
447 "decomposition of one soil C pool is influenced by the dynamics of another soil C pool," also
448 pertains to the structure of some C saturation models we tested in this study. Controlling
449 microbial C use efficiency based on temperature has proven to be an important model feature
450 that improves the representation of temperature effects on C cycling (Allison et al., 2010;
451 Wetterstedt and Ågren, 2011). Given the sensitivity of N mineralization to C use efficiency that
452 we observed in our study, temperature controls on C use efficiency in a model are also likely to

affect a coupled N cycle. A next step in the development of new ecosystem models will be to test how models behave when several new C cycling processes are implemented simultaneously.

5. Conclusions

We demonstrated that different C saturation model structures can produce similar predictions of C storage, but that predictions of N mineralization can diverge widely. Inclusion of a microbial pool in the microbial saturation model led to more reasonable predictions of N mineralization compared to the single-pool saturation model. We also demonstrated that the link between C saturation and N mineralization depends on whether C saturation is modeled as a process regulating transfer efficiencies or transfer rates among pools in the model. In a C saturation model in which the saturation ratio regulates the transfer efficiency, the N mineralization dynamics across a soil texture gradient are similar to that of the non-saturating RothC model. These findings lead to new hypotheses about the relationship between C saturation and N mineralization that can be tested empirically, and offer a clear pathway to represent C saturation and N mineralization dynamics.

References

Allison, S. D., Wallenstein, M. D. and Bradford, M. A.: Soil-carbon response to warming dependent on microbial physiology, Nat. Geosci., 3(5), 336–340, 2010.

Baldock, J. . and Skjemstad, J. .: Role of the soil matrix and minerals in protecting natural organic materials against biological attack, Org. Geochem., 31(7-8), 697–710, 2000.

Castellano, M., Kaye, J., Lin, H., and Schmidt, J.: Linking Carbon Saturation Concepts to Nitrogen Saturation and Retention, Ecosystems, 15, 175-187, 2012.

Eliasson, P. E. and Ågren, G. I.: Feedback from soil inorganic nitrogen on soil organic matter mineralisation and growth in a boreal forest ecosystem, Plant Soil, 338(1-2), 193–203, 2010.

Gulde, S., Chung, H., Amelung, W., Chang, C. and Six, J.: Soil Carbon Saturation Controls Labile and Stable Carbon Pool Dynamics, Soil Sci. Soc. Am. J., 72(3), 605, 2008.

Hassink, J.: Preservation of Plant Residues in Soils Differing in Unsaturated Protective Capacity, Soil Sci. Soc. Am. J., 60, 487, 1996.

Hassink, J.: The capacity of soils to preserve organic C and N by their association with clay and silt particles, Plant Soil, 191(1), 77–87, 1997.

Hassink, J., and Whitmore, A. P.: A Model of the Physical Protection of Organic Matter in Soils, Soil Sci. Soc. Am. J., 61, 131-139, 1997.

Heitkamp, F., Wendland, M., Offenberger, K. and Gerold, G.: Implications of input estimation, residue quality and carbon saturation on the predictive power of the Rothamsted Carbon Model, Geoderma, 170, 168–175, 2012.

Hénin, S., and Dupuis, M.: Essai de bilan de la matière organique du sol, Ann. Agron., 15, 17-29, 1945.

Huggins, D. R., Clapp, C. E., Allmaras, R. R., Lamb, J. A., and Laysee, M. F.: Carbon dynamics in corn-soybean sequences as estimated from natural Carbon-13 abundance, Soil Sci. Soc. Am. J., 62, 195-203, 1998.

Jenkinson, D. S.: The Turnover of Organic-Carbon and Nitrogen in Soil, Philos. T. Roy. Soc. B, 329, 361-368, 1990.

Kemanian, A. R., Manoranjan, V. S., Huggins, D. R., and Stöckle, C. O.: Assessing the usefulness of simple mathematical models to describe soil carbon dynamics, 3rd USDA Symposium on Greenhouse Gases & Carbon Sequestration in Agriculture and Forestry, Baltimore, Maryland, March 21-24, 2005, 2005.

Kemanian, A. R., and Stöckle, C. O.: C-Farm: A simple model to evaluate the carbon balance of soil profiles, Eur. J. Agron., 32, 22-29, 2010.

Kemanian, A. R., Julich, S., Manoranjan, V. S., and Arnold, J. R.: Integrating soil carbon cycling with that of nitrogen and phosphorus in the watershed model SWAT: Theory and model testing, Ecol. Model., 222, 1913-1921, 2011.

Ladd, J. N., Oades, J. M., and Amato, M.: Microbial biomass formed from ^{14}C,^{15}N-labelled plant material decomposing in soils in the field, Soil Biol. Biochem., 13, 119-126, 1981.

Manzoni, S., Jackson, R. B., Trofymow, J. A., and Porporato, A.: The global stoichiometry of litter nitrogen mineralization, Science, 321, 684-686, 2008.

Manzoni, S., and Porporato, A.: Soil carbon and nitrogen mineralization: Theory and models across scales, Soil Biol. Biochem., 41, 1355-1379, 2009.

Manzoni, S., Trofymow, J. A., Jackson, R. B., and Porporato, A.: Stoichiometric controls on carbon, nitrogen, and phosphorus dynamics in decomposing litter, Ecol. Monogr., 80, 89-106, 2010.

Manzoni, S., Taylor, P., Richter, A., Porporato, A., and Ågren, G. I.: Environmental and stoichiometric controls on microbial carbon-use efficiency in soils, New Phytol., 196, 79-91, 2012.

Mazzilli, S., Kemanian, A., Ernst, O., Jackson, R., Piñeiro, G.: Priming of soil organic carbon decomposition induced by corn compared to soybean crops, Accepted in Soil Biol. Biochem.: 2014.

McLauchlan, K. K.: Effects of soil texture on soil carbon and nitrogen dynamics after cessation of agriculture, Geoderma, 136, 289-299, 2006.

Parton, W. J., Schimel, D. S., Cole, C. V., and Ojima, D. S.: Analysis of factors controlling soil organic matter levels in Great Plains grasslands, Soil Sci. Soc. Am. J., 51, 1173-1179, 1987.

Perveen, N., Barot, S., Alvarez, G., Klumpp, K., Martin, R., Rapaport, A., Herfurth, D., Louault, F. and Fontaine, S.: Priming effect and microbial diversity in ecosystem functioning and response to global change: a modeling approach using the SYMPHONY model., Glob. Chang. Biol., 20(4), 1174–90, 2014.

Schimel, D. S.: Carbon and nitrogen turnover in adjacent grassland and cropland ecosystems, Biogeochemistry, 2, 345-357, 1986.

Schimel, J. P. and Weintraub, M. N.: The implications of exoenzyme activity on microbial carbon and nitrogen limitation in soil: a theoretical model, Soil Biol. Biochem., 35(4), 549–563, 2003.

Schmidt, M. W. I., Torn, M. S., Abiven, S., Dittmar, T., Guggenberger, G., Janssens, I. a, Kleber, M., Kögel-Knabner, I., Lehmann, J., Manning, D. a C., Nannipieri, P., Rasse, D. P., Weiner, S. and Trumbore, S. E.: Persistence of soil organic matter as an ecosystem property., Nature, 478(7367), 49–56, 2011.

Sinsabaugh, R. L., Manzoni, S., Moorhead, D. L., and Richter, A.: Carbon use efficiency of microbial communities: stoichiometry, methodology and modelling, Ecol. Lett., 16, 930-939, 2013.

Six, J., Conant, R. T., Paul, E. A. and Paustian, K.: Stabilization mechanisms of soil organic matter: Implications for C-saturation of soils, Plant Soil, 241(2), 155–176, 2002.

Sørensen, L. H.: The influence of clay on the rate of decay of amino acid metabolites synthesized in soils during decomposition of cellulose, Soil Biol. Biochem., 7, 171-177, 1975.

Sørensen, L. H.: Carbon-nitrogen relationships during the humification of cellulose in soils containing different amounts of clay, Soil Biol. Biochem., 13, 313-321, 1981.

Stewart, C. E., Paustian, K., Conant, R. T., Plante, A. F., and Six, J.: Soil carbon saturation: concept, evidence and evaluation, Biogeochemistry, 86, 19-31, 2007.

Stewart, C. E., Plante, A. F., Paustian, K., Conant, R. T., and Six, J.: Soil carbon saturation: Linking concept and measurable carbon pools, Soil Sci. Soc. Am. J., 72, 379-392, 2008.

Stewart, C. E., Follett, R. F., Wallace, J., and Pruessner, E. G.: Impact of Biosolids and Tillage on Soil Organic Matter Fractions: Implications of Carbon Saturation for Conservation Management in the Virginia Coastal Plain, Soil Sci. Soc. Am. J., 76, 1257-1267, 2012.

Van Veen, J. A., Ladd, J. N., and Amato, M.: Turnover of Carbon and Nitrogen through the Microbial Biomass in a Sandy Loam and a Clay Soil Incubated with [^{14}C(U)]Glucose and [^{15}N] $(NH_4)_2SO_4$ under Different Moisture Regimes, Soil Biol. Biochem., 17, 747-756, 1985.

Verberne, E. L. J., Hassink, J., Dewilligen, P., Groot, J. J. R., and Van Veen, J. A.: Modeling Organic-Matter Dynamics in Different Soils, Neth. J. Agr. Sci., 38, 221-238, 1990.

Wetterstedt, J. Å. M. and Ågren, G. I.: Quality or decomposer efficiency – which is most important in the temperature response of litter decomposition? A modelling study using the GLUE methodology, Biogeosciences, 8(2), 477–487, 2011.
Wutzler, T. and Reichstein, M.: Colimitation of decomposition by substrate and decomposers- a comparison of model formulations, Biogeosciences, 5, 749–759, 2008.

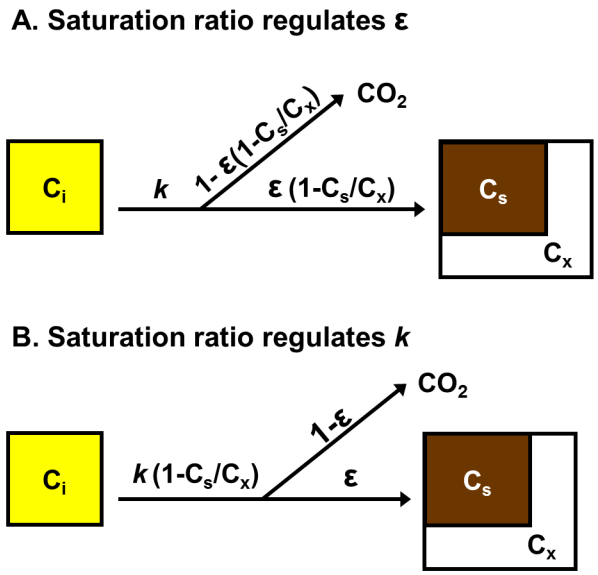

Figure 1. Conceptual models illustrating two different methods of implementing C saturation dynamics. In both models, the C saturation ratio of the saturating pool is defined by the ratio of the current pool size (C_s) to a theoretical maximum pool size (C_x), or C_s/C_x. In model A, the C saturation ratio regulates the C transfer efficiency (ε) between the donor pool (C_i) and C_s. As the C saturation ratio increases, less of the C decomposed from C_i is transferred to C_s and more is respired as CO_2. In model B, the C saturation ratio regulates the decomposition rate (k) of C_i, such that the rate decreases as the C saturation ratio increases. The C transfer efficiency is not affected by the C saturation ratio in model B.

A. Single-pool Saturation

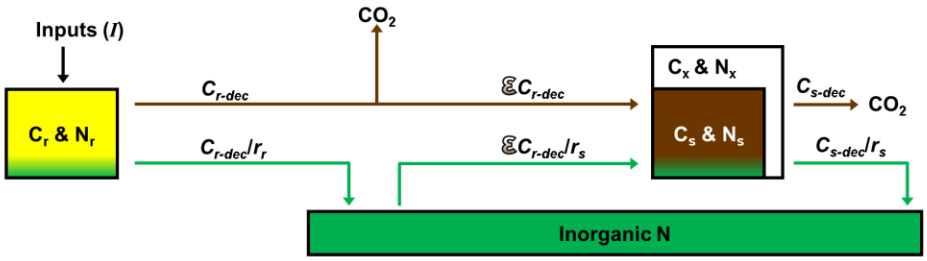

B. Microbial Saturation

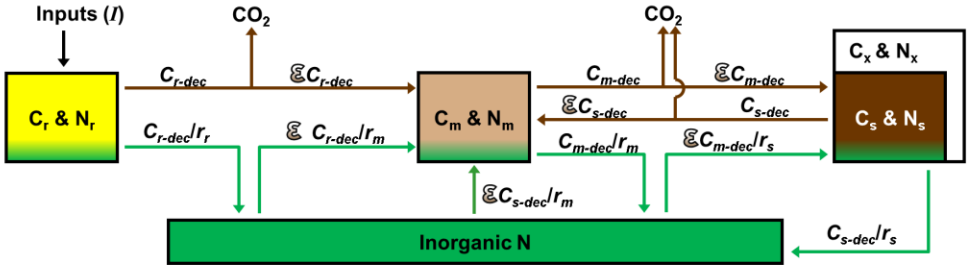

C. Abiotic Saturation

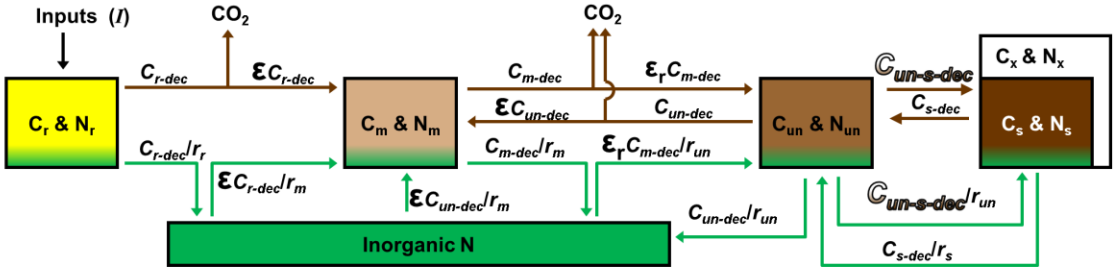

D. RothC

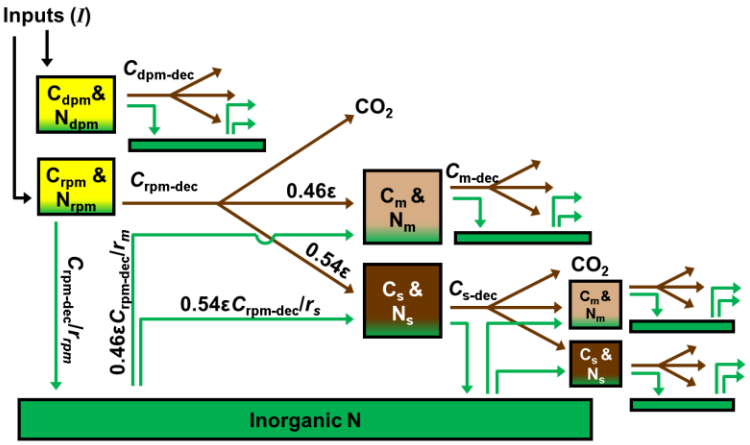

572

573

Figure 2. Diagrams of the pools and fluxes in the four models used in this study. Carbon and N pools are indicated together in boxes. Carbon fluxes are indicated by brown arrows and N fluxes by green arrows. Pools are abbreviated as follows: $C_{r,}$ $C_{dpm,}$ C_{rpm} and $N_{r,}$ $N_{dpm,}$ N_{rpm} are plant residues; C_m and N_m are microbial biomass; C_{un} and N_{un} are un-protected soil organic matter; C_s and N_s are protected or stabilized soil organic matter; C_x and N_x are the maximum or saturating capacity for C and N storage. The inorganic N pool is represented by a green box. Carbon decomposition from each pool and the pool stoichiometry (C:N ratio) are represented by the symbols $C_{j\text{-dec}}$ and r_j, respectively, where j specifies the pool. Pools decompose with first order kinetics based on rates listed in Table 1. The symbol ε is the C transfer efficiency to the receiving pool, the value of which is specified by Table 1 for each model. Symbols illustrated with a brown gradient fill pattern are regulated by the C saturation ratio (C_s/C_x).

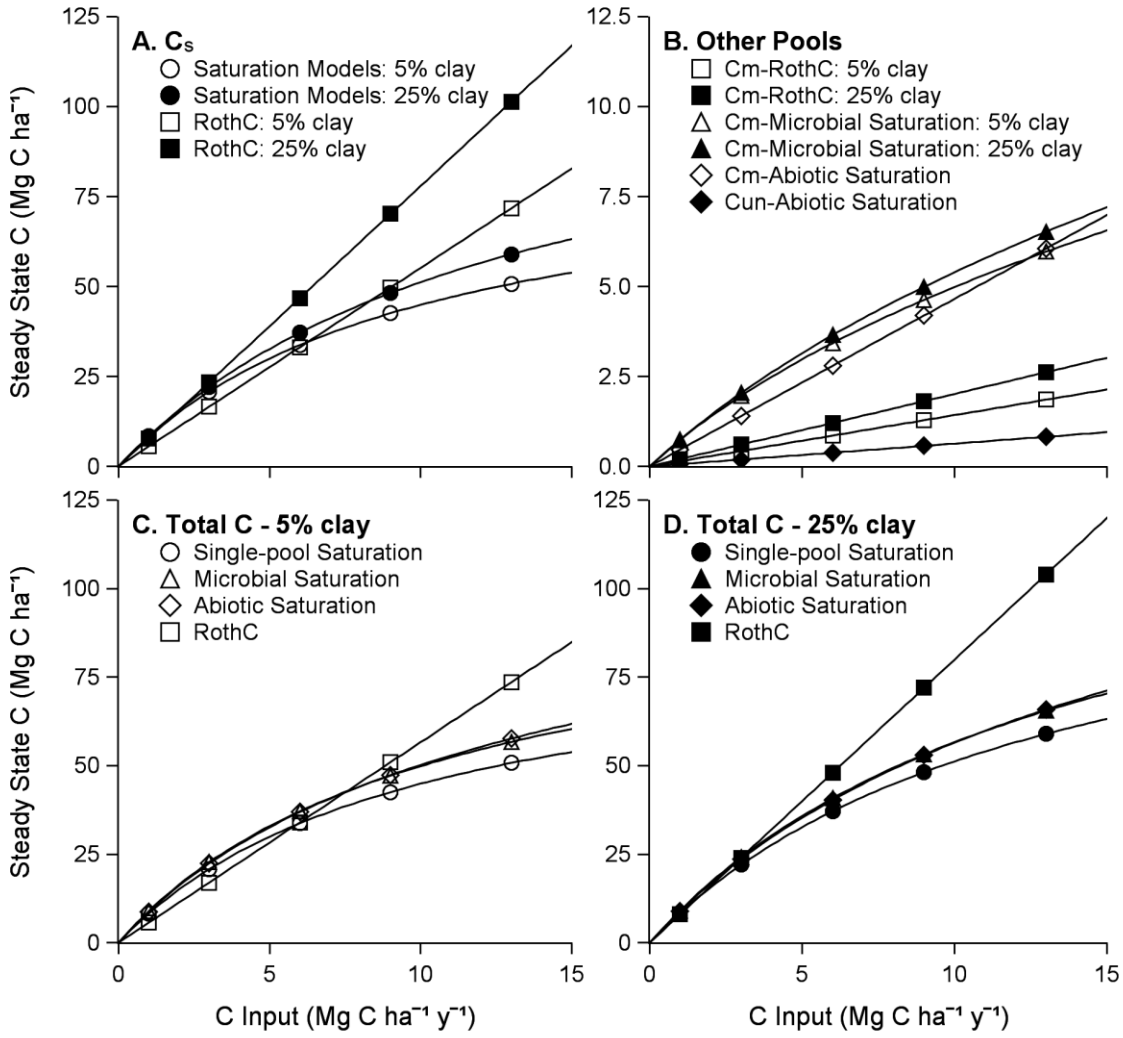

586

587 **Figure 3.** The relationship between C input level and the steady-state C level of various
588 pools in each model for soils with contrasting clay concentration. **(A)** The C_s pool of
589 each model in soils with 0.05 and 0.25 clay concentration. **(B)** Other C pools in each
590 model in soils with 0.05 and 0.25 clay concentration (note: the pools in the abiotic
591 saturation model are not sensitive to clay concentration). **(C, D)** The total C pool size in
592 soils with 0.05 clay concentration **(C)** and 0.25 clay concentration **(D)**.

593

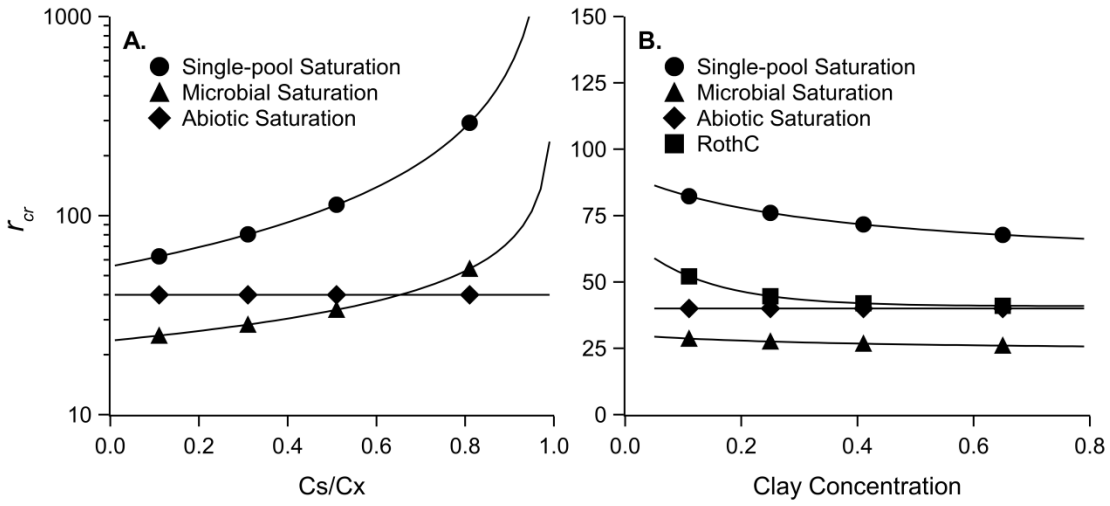

Figure 4. The critical C:N ratio (r_{cr}) as a function of carbon saturation ratio **(A)** and clay concentration **(B)**. In **(B)**, the pool size for C_s was maintained constant at 32 Mg C ha^{-1}, thus the clay gradient creates a C saturation gradient. For reference, a pool size of 32 Mg C ha^{-1} would result from an annual C input level of ~5 Mg C ha^{-1} y^{-1}.

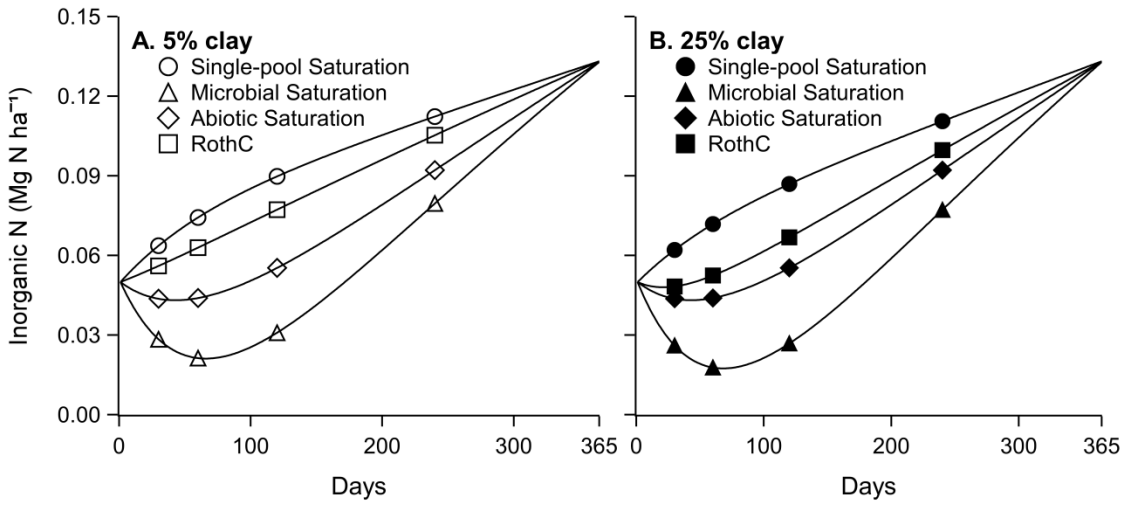

Figure 5. The inorganic N pool during decomposition of a 5 Mg C ha^{-1} residue addition with a *r* of 60 in a soil with 0.05 clay concentration **(A)** and 0.25 clay concentration **(B)**. Soil C pool sizes for each model structure were initialized to the steady state levels that would occur from annual residue additions of 5 Mg C ha^{-1}. Residue and soil C pools decomposed at the optimum rates listed in Table 1.

608 Table 1. The parameter values used in each model.

Parameter	Description	Units	Single-pool Saturation	Microbial Saturation	Abiotic Saturation	RothC
C_x[a]	Maximum capacity of C_s	g C kg^{-1} soil	$21.1 + 37.5f_{clay}$	$21.1 + 37.5f_{clay}$	$21.1 + 37.5f_{clay}$	
ε_x	Humification coefficient	g C g^{-1} C	0.18	0.18	0.18	
ε	Carbon transfer efficiency	g C g^{-1} C	$\varepsilon_x(1 - C_s/C_x)$	$\sqrt{\varepsilon_x(1 - C_s/C_x)}$	0.25	$\frac{1}{4.09 + 2.67e^{-7.86f_{clay}}}$
ε_r	Carbon recycling efficiency	g C g^{-1} C			0.75	
k_r	Residue decomposition rate	d^{-1}	0.0165	0.0165	0.0165	
k_{dpm}	Labile residue decomposition rate	d^{-1}				0.0274
k_{rpm}	Recalcitrant residue decomposition rate	d^{-1}				8.2×10^{-4}
k_s	C_s decomposition rate	d^{-1}	5.48×10^{-5}	$\frac{5.48 \times 10^{-5}}{(1 - \varepsilon^2)}$	$\frac{5.48 \times 10^{-5}}{k_{un}(1 - \varepsilon\,\varepsilon_r)}$	5.48×10^{-5}
k_m	C_m decomposition rate	d^{-1}		1.81×10^{-3}	1.81×10^{-3}	1.81×10^{-3}
$k_{un\text{-}s}$	Transfer rate from C_{un} to C_s	d^{-1}			$\frac{\varepsilon_x(1 - C_s/C_x)}{\varepsilon\,\varepsilon_r}$	
k_{un}	C_{un} decomposition rate	d^{-1}			0.01	

[a]C_x as calculated by Hassink and Whitmore (1997). For use in the modeling exercises, we converted C_x to units of Mg C ha^{-1} by assuming a soil bulk density of 1.3 Mg m^{-3} and a soil depth of 0.3 m.

Table 2. Differential equations for carbon pools in each model.

Single-pool saturation model	
$dC_r/dt = I^a - k_r C_r$	(3)
$dC_s/dt = \varepsilon\, k_r C_r - k_s C_s$	(4)
Microbial saturation model	
$dC_r/dt = I - k_r C_r$	(5)
$dC_m/dt = \varepsilon\, k_r C_r + \varepsilon\, k_s C_s - k_m C_m$	(6)
$dC_s/dt = \varepsilon\, k_m C_m - k_s C_s$	(7)
Abiotic saturation model	
$dC_r/dt = I - k_r C_r$	(8)
$dC_m/dt = \varepsilon\, k_r C_r + \varepsilon\, k_{un} C_{un} - k_m C_m$	(9)
$dC_{un}/dt = \varepsilon_r\, k_m C_m + k_s C_s - k_{un} C_{un} - k_{un\text{-}s} C_{un}$	(10)
$dC_s/dt = k_{un\text{-}s} C_{un} - k_s C_s$	(11)
RothC	
$dC_{dpm}/dt = 0.59I - k_{dpm} C_{dpm}$	(12)
$dC_{rpm}/dt = 0.41I - k_{rpm} C_{rpm}$	(13)
$dC_s/dt = 0.54\, \varepsilon\, (k_{dpm} C_{dpm} + k_{rpm} C_{rpm} + k_m C_m + k_s C_s) - k_s C_s$	(14)
$dC_m/dt = 0.46\, \varepsilon\, (k_{dpm} C_{dpm} + k_{rpm} C_{rpm} + k_m C_m + k_s C_s) - k_m C_m$	(15)

[a] I = Plant residue C inputs

611

Table 3. Analytical solutions to the steady-state level of the SOC pools in each model. Carbon input rate (I) and turnover rates k_s, k_m, and k_{un} must have same time units.

All saturation models

$$C_s = \frac{\varepsilon_x I}{k_s^{a} + \varepsilon_x C_r / C_x} \quad (17)$$

Microbial saturation model

$$C_m = \frac{\sqrt{\varepsilon_x (1 - C_s/C_x)}\ I}{k_m (1 - \varepsilon_x (1 - C_s/C_x))} \quad (18)$$

Abiotic saturation model

$$C_m = \frac{\varepsilon\ I}{k_m (1 - \varepsilon\ \varepsilon_r)} \quad (19)$$

$$C_{un} = \frac{\varepsilon\ \varepsilon_r\ I}{k_{un} (1 - \varepsilon\ \varepsilon_r)} \quad (20)$$

RothC

$$C_s = \frac{0.54 \varepsilon\ I}{k_s (1 - \varepsilon)} \quad (21)$$

$$C_m = \frac{0.46 \varepsilon\ I}{k_m (1 - \varepsilon)} \quad (22)$$

[a]The k_s parameter value from the single-pool saturation model.

612
613

Table 4. The analytical solution to r_{cr} in each model.

Single-pool saturation

$$r_{cr} = \frac{r_s}{\varepsilon_x(1 - \mathrm{C_s}/C_\mathrm{x})} \quad (23)$$

Microbial saturation

$$r_{cr} = \frac{r_m}{\sqrt{\varepsilon_x(1 - \mathrm{C_s}/C_\mathrm{x})}} \quad (24)$$

Abiotic saturation

$$r_{cr} = \frac{r_m}{0.25} \quad (25)$$

RothC

$$r_{cr} = (0.54r_s + 0.46r_m)\,(4.0 + 2.67e^{-7.86\mathrm{f_{clay}}}) \quad (26)$$

Appendix A

Deriving the parameter k_s for the microbial saturation model that would force steady-state C_s levels to be equivalent to the single-pool saturation model required reformulating Eq. (7) to solve dC_s/dt with respect to C_r. This is achieved by solving steady-state Eq. (6) for $k_m C_m$ and substituting this for $k_m C_m$ in Eq. (7). The result is Eq. (A1):

$$dC_s/dt = \varepsilon^2 k_r C_r - (1- \varepsilon^2) k_s C_s \quad \text{(A1)}$$

Eq. (A1) and Eq. (4) can equated and the turnover rate for C_s in model B solved:

$$k_s = \frac{5.48 \times 10^{-5}}{(1 - \varepsilon^2)} \quad \text{(A2)}$$

To derive parameters for the abiotic saturation model that would force steady-state C_s levels to be equivalent to steady-state C_s levels in the single-pool saturation model we reformulated Eq. (11) to solve dC_s/dt with respect to C_r. This required rearrangements of Eq. (10) and Eq. (9) along with several substitutions. First, steady-state Eq. (9) was solved for $k_m C_m$ and substituted into Eq. (10), which was then solved for C_{un}. The resulting equation for C_{un} was substituted into Eq. (11), yielding:

$$dC_s/dt = \varepsilon_r \varepsilon k_{un\text{-}s} k_r C_r - k_{un} (1- \varepsilon_r \varepsilon) k_s C_s \quad \text{(A3)}$$

Eq. (A3) and Eq. (4) can be equated and the decay rates $k_{un\text{-}s}$ and k_s solved:

$$k_{un\text{-}s} = \frac{\varepsilon_x (1 - C_s/C_x)}{\varepsilon \, \varepsilon_r} \quad \text{(A4)}$$

$$k_s = \frac{5.48 \times 10^{-5}}{k_{un}(1 - \varepsilon\, \varepsilon_r)} \quad \text{(A5)}$$

633